

Optimization of mass spectrometers using the adaptive particle swarm algorithm

A. Bieler,* K. Altwegg, L. Hofer, A. Jäckel, A. Riedo, T. Sémon, P. Wahlström and P. Wurz

Optimization of mass spectrometers using the adaptive particle swarm algorithm (APSA) is described along with implementations for ion optical simulations and various time-of-flight (TOF) instruments. The need for *in situ* self optimization is addressed through discussion of the reflectron TOF mass spectrometer (RTOF) on the European Space Agency mission Rosetta. In addition, a tool for optimization of laboratory mass spectrometers is presented and tested on two different instruments. After the application of APSA optimization, a substantial increase in performance for mass spectrometers that have manually been tuned for several weeks or months is demonstrated. Copyright © 2011 John Wiley & Sons, Ltd.

Keywords: particle swarm optimization; Rosetta; SIMION; 67P/Churyumov-Gerasimenko

INTRODUCTION

Mass spectrometry is a powerful tool in space research. Whereas the earliest mass spectrometers flown on spacecraft were mainly designed to measure plasma (e.g. magnetosphere^[1] and solar wind^[2]), contemporary missions also carry mass spectrometers to analyze neutrals, ions and dust in cometary coma.^[3,4] The atmosphere of Titan,^[5] geysers of Enceladus^[6] or ice and organic material on a comet nucleus^[7,8] are all examples of field applications of mass spectrometry in space science.

Furthermore, future space missions like Phobos-Ground, Luna Resource or Luna Glob will also investigate surface material using the time-of-flight (TOF) mass spectrometry concept coupled with a laser ablation ion source.^[9–12] The early mass spectrometers flown were mostly either classical electrostatic/magnetic sensors or quadrupole mass spectrometers, these designs are now more frequently replaced by TOF instruments (e.g. Ulysses-SWICS,^[2] COSIMA,^[4] COSAC,^[8] ROSINA-RTOF,^[3] LAZMA^[9]).

In general, TOF instruments operate by pulsed extraction of all ions from the ionization region into a drift tube forming narrow ion packets. All ions are simultaneously accelerated to the same energy and hence differ in velocities according to their mass. TOF instruments have the advantage of taking a spectrum over the whole mass range during one single extraction. One reason to use TOF instruments in space is their relatively simple mechanical design and easy operation, since their performance depends on fast electronics rather than on mechanical tolerances.

In order to get an optimal ion optical design for the specific purpose of the mass spectrometers (dust analysis, high energy plasmas, neutral atmospheres, etc.), which has to be adapted to the available volume and mass, very often ion optical simulation software (e.g. SIMION[®]) is used. The design of ion optical elements like lenses, ion sources, ion mirrors is then optimized to get a high mass resolution combined with a high sensitivity and transmission. Finding the ideal technical solution is nevertheless rather cumbersome as there are a lot of interdependencies between the ion optical elements. Once the hardware has been produced the appropriate operation voltages have to be found

for these elements. Solutions obtained with SIMION serve as starting point. However, as no simulation will perfectly reproduce the behaviour of the final instrument (e.g. SIMION does not support space charge effects up to version 8.1), further tuning on the hardware itself is needed to get maximum performance. This is normally done by tuning the voltages of electrodes manually to maximize the performance of the instrument. Due to the large number of voltages, which are very often dependent on each other, and the high level of precision required for these voltages, this optimization process is a very tedious job.

In this paper, we describe a method which can be used to first optimize the geometrical design of a mass spectrometer within SIMION and then optimize the operation of the manufactured sensor by the same algorithm.

In this way, many optimization steps for the design of the sensor can be done in a relatively short time before producing hardware. After production, the performance of the instrument can be optimized during operation to take into account any differences between modelled and real hardware. This optimization can even be done after launch in space to account for shortcomings in the electronics or for temperature or ageing effects.

This method is currently used to re-optimize the ROSINA-RTOF sensor after a high voltage failure, to design new mass spectrometers for future missions and to tune a novel type of miniaturized laser TOF mass spectrometer (LMS) designed for *in situ* high sensitivity and precision surface composition measurements for future space missions.

RTOF instrument

In March 2004, the European Space Agency (ESA) launched the Rosetta spacecraft onboard an Ariane-5 G+ rocket. Rosetta will

* Correspondence to: Andre Bieler, Universität Bern, Physikalisches Institut, Sidlerstrasse 5, 3012 Bern, Switzerland. E-mail: bieler@space.unibe.ch

Physikalisches Institut, University of Bern, CH-3012 Bern, Switzerland

perform scientific measurements at the comet 67P/Churyumov-Gerasimenko starting from May 2014 until the end of the mission in December 2015. During this time, Rosetta will accompany the comet in close vicinity on its way towards perihelion (1.28 AU) and out again. The Rosetta orbiter's scientific payload includes 11 scientific instruments; the lander Philae carries an additional ten scientific instruments. One of the orbiter instruments is the Rosetta Orbiter Sensor for Ion and Neutral Analysis (ROSINA) which is designed to measure the neutral and ionized volatile material in the coma of the comet. The ROSINA instrument suite consists of a COmetary Pressure Sensor (COPS) and two mass spectrometers. One is a classical Double Focussing Mass Spectrometer (DFMS) with a very high mass resolution ($m/\Delta m = 3000$ at 1% peak height). It covers a mass range from 12 to 150 amu/q. DFMS is able to detect particle densities down to 1 cm^{-3} in less than 20 s, however, only for one mass at the time. The second mass spectrometer is a reflectron-type TOF (RTOF) sensor. It has an extended mass range from 1 to >300 amu/q and records a spectrum of the entire mass range at once. The mass resolution for the present optimized situation is $m/\Delta m \approx 1000$ at 50% peak height. For a complete spectrum, RTOF detects particle densities within a dynamic range of 2–3 decades for an acquisition time of 200 s.

The RTOF ion optics includes four main components (see Fig. 1): ion source, reflectron, hard mirror and detector. It consists of two channels, each containing its dedicated ion source and a detector, but sharing the reflectron. This configuration allows to measure primary ions and neutrals simultaneously. One ion source (electron impact storage ion source) is optimized to measure the cometary neutrals, the other (orthogonal extraction ion source) measures the primary cometary ions. The storage source stores the continuously produced ions and extracts them periodically. The ions fly through the field-free drift region, enter the reflectron where they are reflected and travel back impacting on the storage source detector. The ions in the orthogonal source are extracted without storing them, fly through the field-free drift tube, enter the same reflectron and finally hit the orthogonal detector. For the ion flight trajectory there are 11 voltages (lenses, repellers, grids, etc.) to be adjusted and fine-tuned for the storage source and 15 voltages for the orthogonal source. In order to get a longer flight path and therefore an enhanced mass resolution, the ions can be reflected not only once but three times, twice by the reflectron and once by the hard mirror (see Fig. 1). In this case, the number of parameters to be adjusted increases by two additional voltages of the hard mirror.

RTOF operation in space/need for re-optimization

After the Rosetta launch in March 2004, a commissioning phase took place during which each instrument was switched on carefully. During this first check-out, the ROSINA instruments showed nominal behaviour. However, in autumn 2004, the first anomalies

in the ROSINA-RTOF occurred. At that time, the cause for the anomalies, which consisted in unexpected instrument mode changes, was not understood. One year after launch, a failure in the main 9 kV high voltage converter limited the high voltages to less than 3000 V.

After intensive and prolonged investigations in the laboratory, the cause of the RTOF failure was found to be outgassing in the potting near the high voltage converter leading to partial discharges along some of the potted cables. Subsequently, RTOF was not operated for almost four years in order to not damage the instrument further. Finally, in spring 2010, a software solution was implemented which fixed the maximum output voltage of the high voltage converter to 2 kV. It has been shown in space that with this voltage, RTOF can be operated continuously without any problems. However, this requires that all ion optical elements must be operated with much lower voltages as originally intended. The necessary voltages have been deduced from the spare RTOF model in the laboratory, but the performance in space compared to the one in the laboratory shows that they are not yet fully optimized.

During the rendezvous maneuver between Rosetta and Churyumov-Gerasimenko in May 2014, the one-way signal travel time will be approximately 35 min. It is clear that the instruments have to perform autonomously at these distances from the Earth. Additionally, the long signal travel time in spring 2014 excludes a non- or semi-automatic optimization of all voltage parameters.

Even without failure, it has to be expected that the temperatures will be very low at the start of the mission in 2014 at approx. 3.75 AU from the Sun. It is therefore not clear what the performance of the mass spectrometer under these conditions will be. Later in the mission, the distance to the Sun will become much smaller, temperatures will get much higher and the instrument parameters may have to be retuned. Due to the drastic changes in voltage settings because of the failure and the long mission duration with very different temperature conditions, an autonomous in-flight optimization algorithm is definitely needed. This in-flight optimization algorithm will be described and illustrated in subsequent sections.

The optimization software will be uplinked to the Rosetta spacecraft in 2014, after its hibernation phase has ended, to allow in-flight self-optimization of the mass spectrometer.

Particle swarm optimization

The particle swarm optimization (PSO) algorithm belongs to the class of direct search methods, used to find an optimal solution to a fitness function in a multidimensional search space I . I is an arbitrary interval of the real numbers \mathfrak{R}^D . PSO is derivative free as it is affected by the value of the fitness function only. Introduced in 1995 by Kennedy and Eberhart,^[13] PSO uses simple search operations to mimic swarm behaviour as can be observed in nature. The swarm itself consists of several particles, where

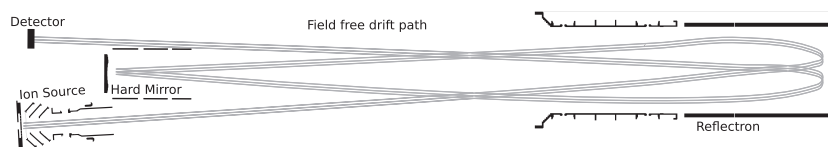


Figure 1. RTOF ion optical design. In triple reflection mode, ions produced in the ion source are reflected twice inside the grid-free reflectron and once in the hard mirror.

one particle X_i represents a possible solution to the problem. $X_i = [x_i^1, x_i^2, x_i^3, \dots, x_i^D]$ with upper indices referring to dimension and the lower ones to particle number. After every iteration step, the fitness function $f: \mathfrak{R}^D \rightarrow \mathfrak{R}$ is evaluated for all particles, representing their fitness as a single number. The quality of a solution candidate X_i depends on the value of its fitness function only; the lower the number, the better the solution.

Every particle has a memory where two solutions are stored. One is the best solution that has been found by the whole swarm \tilde{X} , the other the particle's own best solution $X_{i(best)}$.

The position at iteration k of particle number i is calculated according to

$$X_i^{k+1} = X_i^k + \Delta X_i^k$$

and the displacement vector as

$$\Delta X_i^k = \omega \cdot \Delta X_i^{k-1} + S_i + C_i$$

with the social and cognitive terms S_i and C_i ,

$$S_i = c_1 \cdot R_{1,i}^k \cdot (\tilde{X} - X_i^k)$$

$$C_i = c_2 \cdot R_{2,i}^k \cdot (X_{i(best)} - X_i^k)$$

$R_{1,i}^k$ and $R_{2,i}^k$ are vectors with randomly uniform distributed elements from 0 to 1, generated for every iteration step. Convergence speed is mainly influenced by $\omega < 1$ as it adds to ΔX_i^k a fraction of the displacement vector from the previous iteration $k-1$. The social and cognitive weighing parameters c_1 and c_2 , respectively, control the way particles move towards their own best or the global best solution.

Parameter tuning and adaptive particle swarm optimization (APSO)

Besides the global version of PSO described above (GPSO), there are many other variations of this algorithm because it is easy to implement and is basically controlled by the three parameters ω , c_1 and c_2 . Consequently, a lot of recent work has been done on parameter tuning of PSO algorithm as different sets of ω , c_1 and c_2 lead to varying performance depending on the optimization problem.

Zhan *et al.*^[14] introduced a promising approach with an adaptive PSO technique, a GPSO derivative with parameter tuning done at run time. Four evolutionary states of the swarm are distinguished, based on the distribution of the particles inside the search space.

Depending on evolutionary state, ω , c_1 and c_2 are adapted dynamically. In addition, there is an elitist learning mechanism, allowing the swarm jumping out of a local minimum. For this purpose, a solution candidate is created from the best current solution \tilde{X} , varying in only one (randomly chosen) dimension. This mechanism is similar to mutation in genetic algorithms. APSO has higher convergence speed as GPSO but is still able to perform global optimization over a wide search space. A more detailed description of APSO can be found in ref.^[14]

OPTIMIZER IMPLEMENTATION

All optimizer specific software has been written in the Python programming language with the application and UI framework Qt, allowing cross platform execution on Windows, Linux and Mac OS. A functional block diagram of a typical optimization process can be seen in Fig. 2.

SIMION optimizer

SIMION is commercial software for calculating electric/magnetic fields and charged particle trajectories by solving the Laplace equation (no space charge), with electrodes defining boundary conditions. It is used for the design and development of ion optical instruments, including mass spectrometers. SIMION optimizer can either be used to optimize voltage settings of already existing SIMION models to improve performance, or to change the geometry of modelled instruments as well, leading to more efficient/simpler designs. The optimization software is not a replacement for, but works on top of SIMION by controlling it through its command line interface. All calculations are done in SIMION with the different parameters (voltages, geometrical factors) provided from APSO.

Implementation of existing SIMION models to the optimizer software takes typically less than 1 h. More complex instruments can be divided into several subsystems (potential arrays or PAs), omitting field-free regions (i.e. drift tubes) and decrease memory requirements of the model. Two operating modes are available, one for voltage optimization only, the other also optimizing the instrument's geometry. Fitness of a specific geometry is determined by a corresponding voltage optimization.

A voltage optimization result for a fairly complex ion optical model with low quality initial settings is shown in Fig. 3, with the fitness function defined as

$$f = -\text{transmission} \cdot \text{mass resolution}$$

For each simulation, 1000 ions were launched inside the ionization region of the ion source. Transmission is defined as the ratio of total created ions over ions arriving at the detector electrode. Mass resolution is calculated from the standard deviation σ_{tof} of the TOF values and $FWHM = 2\sqrt{2 \ln(2)}\sigma_{tof}$. For the problem shown in Fig. 3, only the positions of the PAs relative to each other were modified. This shows only a pseudo geometry optimization since there is no need for refining (solving the Laplace equation) of the new configuration. Real geometry optimization contains a change of shape inside a potential array where subsequent refining is necessary.

To get a more powerful system, parallel computing is introduced in terms of a classical master/slave configuration (Fig. 4). The master node, containing the optimization software, writes solution candidates to a MySQL database as jobs. A job consists of a set of voltages that has to be run in a simulation. Working nodes, where all SIMION calculations are done, autonomously check by network connection the database for open jobs and process them if one is found. Corresponding jobs are then blocked for all other working nodes. Quality of such a simulation is expressed as a fitness and written back to the database by the slave node. When all jobs for one iteration are processed, the master node collects the fitness values and creates new jobs according to the APSO algorithm. The number of working nodes is not limited, and one can thus take full advantage of parallelizing APSO. There is no more gain in performance if the number of working nodes exceeds the number of particles of the swarm, as one job cannot be split among different slaves.

A blocked but not finished job is reopened by the master node after a definable amount of time, avoiding single point failure structure (e.g. the crash of a slave node during a simulation run). Graphical visualization of the optimization progress is important. With this feature, unrealistic fitness function values (e.g. resulting

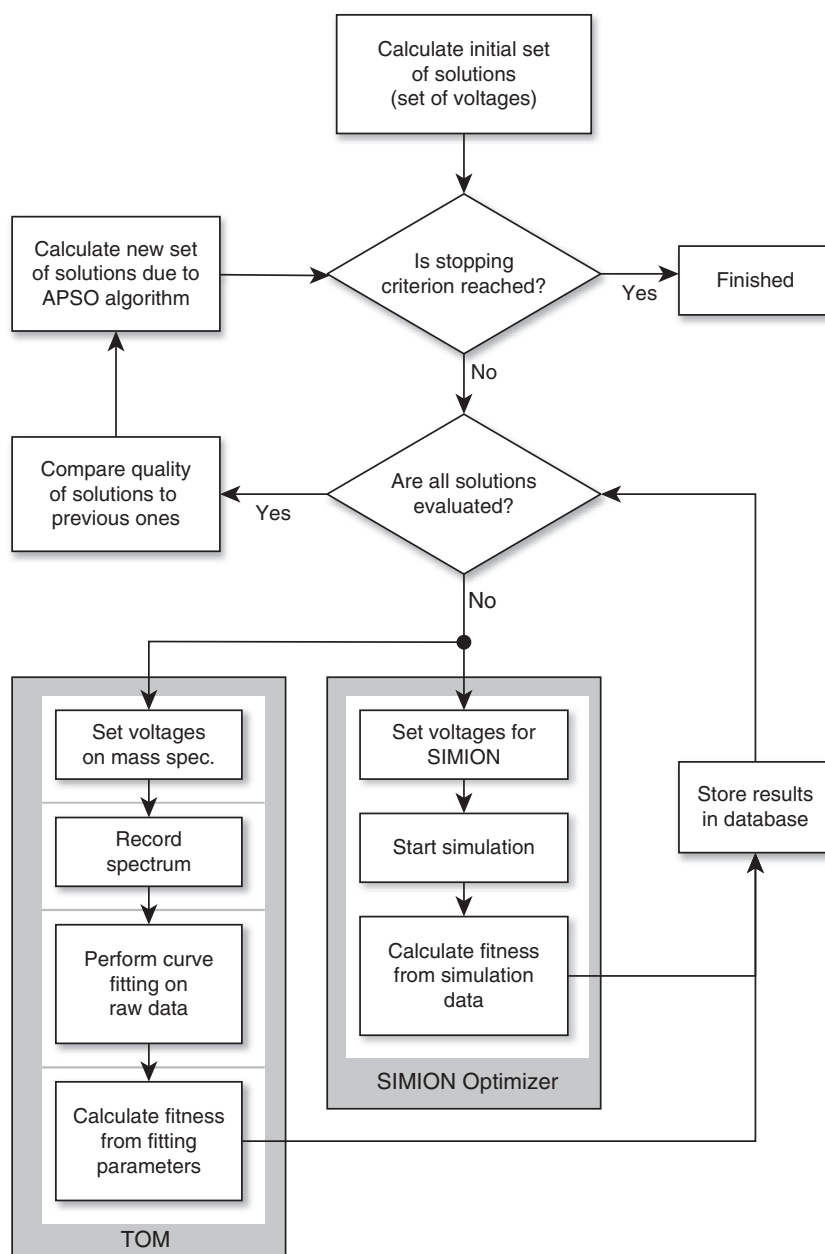


Figure 2. Functional block diagram of the optimization process. The same procedure can be used for tuning hardware with TOM or simulated instruments with SIMION optimizer.

from incorrect SIMION models) and/or unfeasible solutions can be easily identified, and the optimization may be stopped at an early stage.

With increasing complexity of ion optical models, manual optimization thereof becomes very time consuming. With the current configuration of parallel computing where 16 cores are used for the calculations, time consumption for tuning complex SIMION models (say with 15 to 30 different electrodes to adjust) can be reduced from days/weeks to hours. Once started, the whole tuning process runs without the need of any user interaction.

RTOF optimizer

Control of the flight spare RTOF instrument is managed by the Ground Support Equipment Operating System (GSEOS, Fig. 5), a

software package designed to simulate the spacecraft's interface with the onboard instrument.

All the electrodes are selectable for optimization. The best results are generally achieved when all electrodes are involved. For safety reasons search space is separately limited for any electrode. The optimizer software writes parameters (voltages and acquisition time for the spectrum) to an ASCII file which is processed by GSEOS and sent as RTOF commands to the instrument. By defining a specific range of data, different species inside a spectrum may be used for optimization. A single peak Gauss fit is performed on the specified dataset to calculate fitness of the given solution. If multiple peaks appear in the dataset, minor peaks are neglected, and the peak fitting (optimization) is performed on the dominant peak only.

A special feature for RTOF optimization is the introduction of a reference particle to the swarm. This reference particle holds the best parameter set found so far and is evaluated as the last

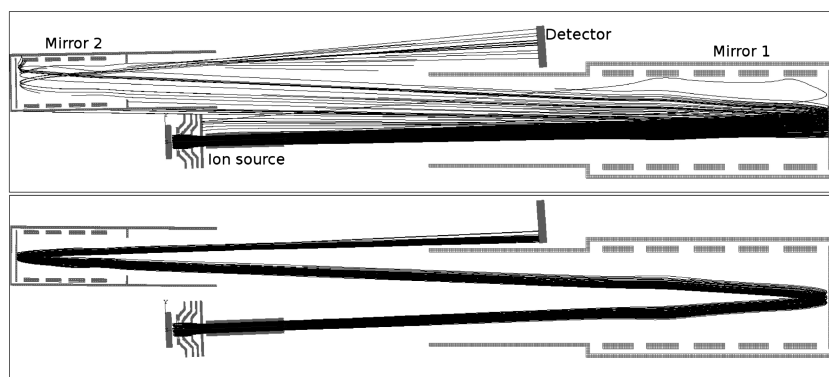


Figure 3. Example of an ion optical simulation with SIMION, consisting of four sub units (Ion Source, Mirror 1 and 2 and the Detector). Ion trajectories are shown in black before and after optimization. Voltage optimization has been performed on all electrodes but the enveloping electrodes of the mirrors. Note that also the position of Mirror 2 has changed during optimization as it has been shifted away from the Ion Source. Additionally, the tilting angle of the Ion Source varies from the initial position.

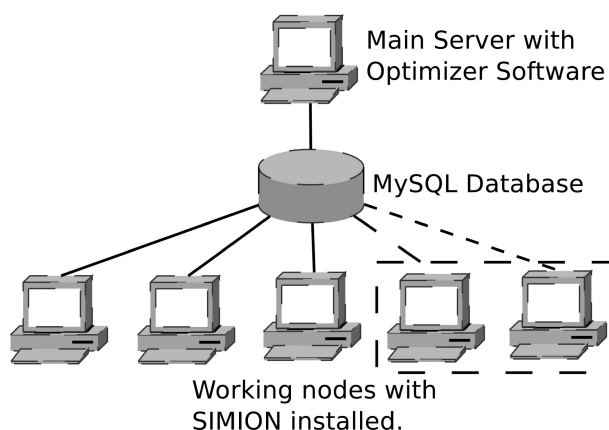


Figure 4. If complexity of the problem is too high for the current configuration, the number of working nodes attached to the MySQL database can be increased without any changes to the software.

particle in every iteration step. In such a way, fitness of the best solution is recalculated permanently. Optimization will therefore still be successful if the target peak dynamically changes over time. In contrast to SIMION optimizer, where high computational power is used (mainly to enhance simulation speed), RTOF optimizer works on an Intel Pentium III CPU with 850 MHz. Typical optimization times are in the range of several hours. Computational power usually is no bottleneck for instrument optimization as the time needed to record a spectrum (60 to 100 s) is much longer than data processing.

Tool for optimizing mass spectrometers (TOM)

Based on the RTOF optimizer package, the more universal TOM for laboratory mass spectrometers was developed. Consisting of a GUI to the optimization software, a remotely controllable power supply and a data acquisition system, it represents a fully equipped framework for optimization of a wide range of mass spectrometers. The power supply unit provides control over eight low-, ten mid- and six high voltage sources via RS-232 interface, having a ± 50 V, ± 500 V and ± 5000 V range, respectively. TOM has three modes of operation:

In control mode, the user simply commands voltage settings to the power supply. Different sets of voltages can be stored on the

host computer and reloaded for later use enabling quick changes between different instrumental operation modes.

Single or multiple electrodes can be examined in scan mode. Selected electrodes are scanned within a user-defined range of voltages, and the instrument's performance (from a defined fitness function) is plotted versus electrode voltage. These plots may then be used to identify critical and/or steady regions of instrument performance dependent on the electrodes.

In optimizer mode, APSO is performed on a user-defined mass range and custom fitness function. TOM has been tested on two different instruments, a linear TOF MS with an orthogonal ion source (LTOF) and a LMS (Laser Mass Spectrometer). Results and instruments are discussed below.

On a graphical user interface, one defines the starting voltages of the optimization as well as the upper and lower limits for every electrode, the maximum number of iterations, the population size of the swarm and the region of the spectrum to be evaluated during optimization.

Test voltages calculated by the APSO algorithm are then commanded by the RS-232 serial port to the power supply unit. Once all voltages are set a spectrum is recorded and stored as an ASCII file. A single peak fit is performed on the highest peak of the dataset, with a user-defined fitting function (*fit*). Fitness (*f*) is then calculated from parameters of the fitting function itself (in the majority of cases, a combination of peak width and amplitude). Fitness and corresponding voltages are stored into a MySQL database. All fitted curves are stored as graphic figures and ASCII-data files together with the original spectrum.

Penalty functions and peak fitting

Penalty functions are introduced to avoid undesired optimization effects resulting from noise in the dataset and/or incorrect curve fitting. As an example, mass resolution is calculated from the width of the fitted (gauss) curve. Hence, single bin noise peaks (i.e. from an analog to digital converter (ADC)), due to their very narrow shape, represent very good solutions to the optimization problem but are not reasonable.

Therefore, a minimum peak width σ_{\min} is defined and peaks with $\sigma < \sigma_{\min}$ are considered noise and ignored. Fitness of such a solution is set to 0, the worst possible value. The same applies for peaks with their peak centers lying outside or at the border of the defined dataset. Because this allows the fitting routine to

search for undesirable solutions and possibly misleads the optimization process.

APSO is very stable concerning penalty functions. Convergence speed may decrease if the frequency of false detections is above approximately 10%.^[15] However, this frequency tends to be lower than 1%, and APSO performance is hardly affected.

RESULTS

RTOF with TOM

In this paragraph, we demonstrate how the self-dependent optimization algorithm contributes to the formidable improvement of the RTOF performance with regard to the 11, resp. 15 voltages to be adjusted and fine-tuned for the storage or orthogonal source, respectively. Furthermore, a significant advantage of the optimization algorithm is the time-saving in comparison to the time-consuming fine-tuning of these voltages by manual optimization, which is not possible in space anyway.

The RTOF instrument has been optimized using H₂O and ⁸⁴Kr mass lines in both single and triple reflection mode with the following functions defined

$$fit = A \cdot \exp\left(-\frac{1}{2} \left(\frac{t - t_0}{\sigma}\right)^2\right) + B$$

Boundary conditions such as initial voltages, upper and lower limits for the electrodes, initial swarm size (population number and spatial distribution) and the acquisition time are defined. After the decision concerning the choice of a target function, the actual optimization is started.

Single reflection mode for a new drift voltage of -1800 V instead of nominal -3000 V has successfully been optimized as can be seen from Figs. 6 and 7. Although peak shapes still differ from a pure Gaussian distribution, these aberrations were decreased to the percent level. After optimization, the mass resolution, which is defined as $m/\Delta m$ at full-width half maximum (FWHM) of the peak, was almost doubled in the single reflection mode. Peak width decreased from 15 ns to 7 ns FWHM (mass 18) and from 30 ns to 17 ns (mass 84). Concerning peak intensities, the water peak at mass 18 [amu/q] is four times larger in the optimized spectrum compared to the not optimized one. For Krypton at mass 84 [amu/q], the intensity increased by a factor of 2.5. Not only mass resolution, peak intensities and peak width were improved by this

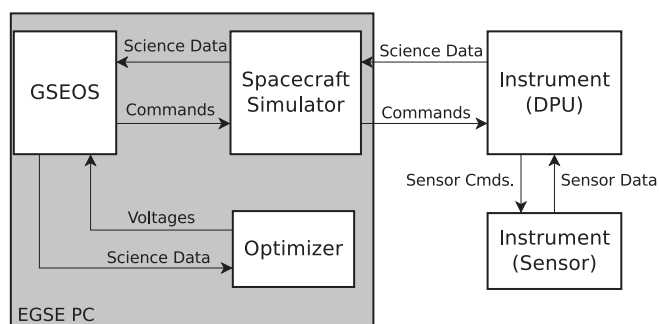


Figure 5. GSEOS overview: Only interactions relevant for optimization software are shown.

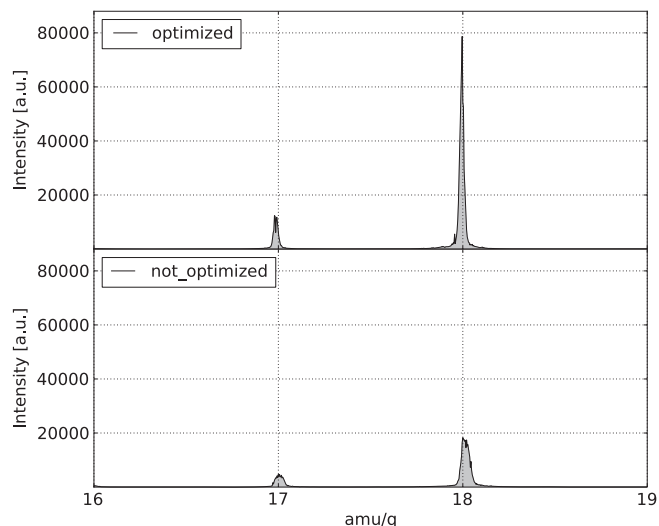


Figure 6. Optimization results for water group peaks with RTOF in single reflection mode.

optimization process, but also the sensitivity could be increased by nearly a factor of two. The sensitivity (S) is defined as follows

$$S = \frac{Area}{t \cdot p \cdot I_{Em}}$$

with the area of the fitted peak, I_{Em} the filament emission current, t the data acquisition time and p the pressure within the ion optical system. Note that the sensitivity differs from its standard definition as it is additionally divided by the emission current of the ion source. For RTOF, there are three different emission current modes with $I_{Em} = 2 \mu A$, $20 \mu A$ and $200 \mu A$, respectively. The science requirements ($m/\Delta m > 500$, mass range > 300 amu/q) are easily met after the optimization process.

Figure 8 shows a typical graphical output during optimization visualizing the evolution of a swarm consisting of ten particles. Within 35 iteration steps (which correspond to 350 recorded spectra), fitness has increased by approximately an order of magnitude. With a data acquisition time of 90 s per spectrum, this corresponds roughly to 9 h of run time.

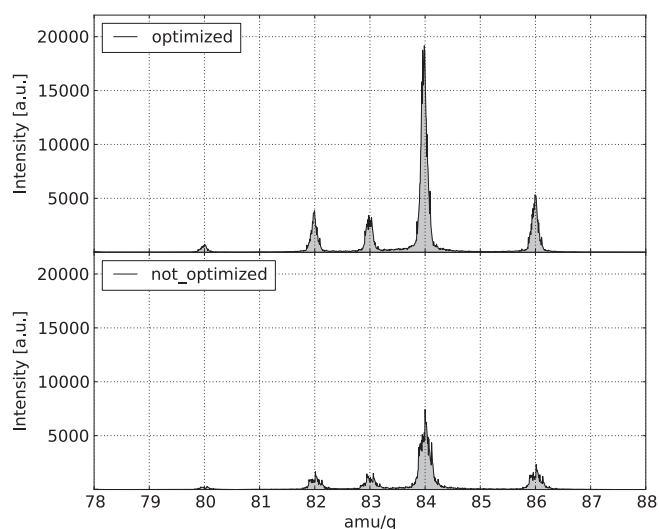


Figure 7. Optimization results for Kr isotopes with RTOF in single reflection mode.

LTOF with TOM

LTOF is a linear TOF mass spectrometer with an orthogonal ion source (see Fig. 9). Neutrals are ionized by electron bombardment and accelerated to approximately 10 eV.

A -300 V extraction pulse then deflects the ions orthogonal to their velocity vector into the TOF section. Additional electrodes further accelerate and focus the beam to -3 keV before it enters a 200-mm drift tube. For ion detection, a chevron multi-channel plate (MCP) detector is used.^[16,17]

For fitting of the LTOF mass lines, a standard Gauss curve was chosen.

$$fit = A \cdot \exp\left(-\frac{1}{2} \left(\frac{t - t_0}{\sigma}\right)^2\right) + B$$

with A , t_0 , σ and B as fitting parameters from which a fitness function can be defined. The aim is an increase of resolution and sensitivity; hence, a fitness function is defined by a combination of A and σ .

$$f = -A/\sigma$$

Figure 10 shows the result of an example optimization. Mass resolution of the LTOF instrument was increased from $m/\Delta m = 40$ to $m/\Delta m = 150$ (both FWHM), and intensity roughly increased by

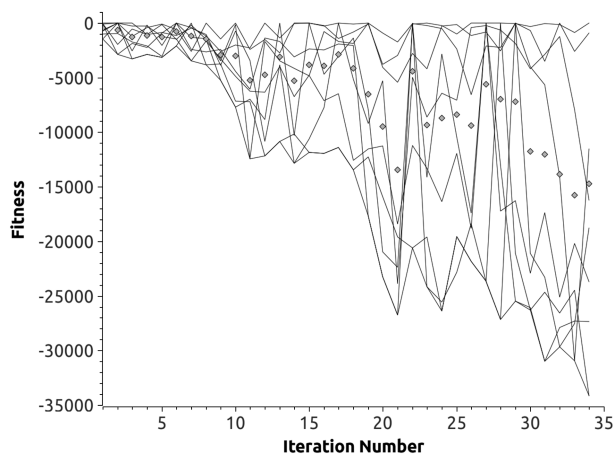


Figure 8. Visualization of the optimization progress with the RTOF instrument. Each line shows the different fitness achieved for one specific particle, with more negative values corresponding to better solutions. Diamonds represent average fitness of the whole swarm.

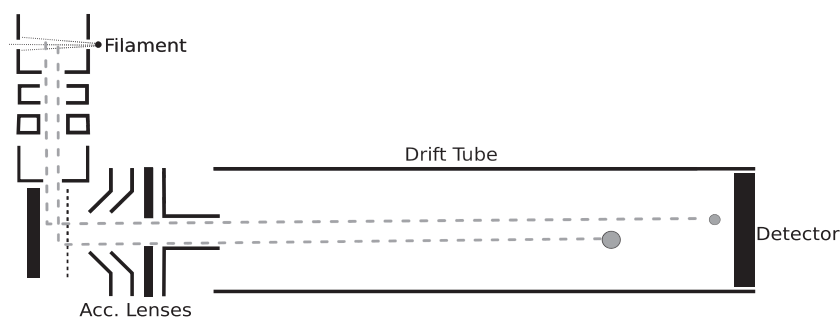


Figure 9. Schematic of LTOF instrument. Ions created by electron impact ionization are accelerated towards an extraction grid. Pulsed with -300 V at typically 5 kHz, the extraction grid accelerates narrow ion packets into the time-of-flight section.

a factor of 10. By optimizing the LTOF instrument manually, only about half of the increases in sensitivity and resolution were reached after many hours of tedious operation.

LMS with TOM

LMS is a laser TOF mass spectrometer using a Q-switched Nd:YAG laser system with a wavelength of 266 nm, pulse length of about 4 ns and has a repetition rate of 20 Hz (see Fig. 11). The pulsed laser beam enters the mass spectrometer by passing the optical lens for beam focusing, propagates through the reflectron and the central hole of the detector assembly and finally reaches the sample by passing the ion optical components.

After material ablation, a plasma plume, containing atomized and ionized species, is formed. A fraction of the positive ions enters the analyzer through the conical nose piece. From there on, these ions are accelerated, confined, collimated and, after travelling the field-free region, are reflected back towards the detector by the reflectron. The detector consists of an assembly of two stacked MCPs in a chevron configuration.

The resulting electron current, generated by the MCP plates, is finally collected by concentric anode rings and sent to a fast acquisition ADC card.

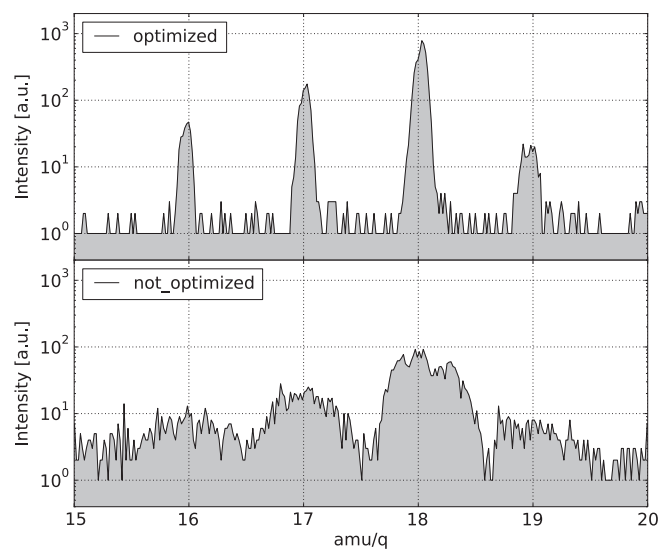


Figure 10. Optimization results for water group peaks with LTOF. Instrument sensitivity increased approximately an order of magnitude and mass resolution by a factor of 4.

LMS is designed, among others, to detect sub-ppm trace elements and has a typical instrumental resolution (measured at FWHM) of about 500–600. Further detailed information can be found in [18].

For optimization of the LMS instrument, a dual fitness function was defined.

$$f = \begin{cases} -A \frac{T}{2 \cdot \Delta T} & \forall A < A^* \\ -A^* \frac{T}{2 \cdot \Delta T} & \forall A \geq A^* \end{cases}$$

where ΔT is the FWHM of the fitted curve, and A the peak amplitude. At the beginning of the optimization process where sensitivity of the instrument is still low, intensity and mass resolution are increased. However, if intensity has increased to the desired value ($A \geq A^*$), only mass resolution is subject to optimization. This is important for very abundant species, preventing the detection system from saturating and instead preferring higher resolution configurations. In the same way, a mass resolution threshold can be defined; once above this threshold, only sensitivity is optimized.

Before optimization, the peak shapes of LMS measurements are not symmetric; therefore, an exponentially modified Gauss curve was selected to fit the raw data.

$$\text{fit} = a \cdot \exp\left(\frac{1}{2} \left(\frac{\sigma}{\tau}\right)^2 - \frac{t-t_0}{\tau}\right) \cdot \left[\text{erf}\left(\frac{1}{\sqrt{2}} \left(\frac{t_0}{\sigma} + \frac{\sigma}{\tau}\right)\right) + \text{erf}\left(\frac{1}{\sqrt{2}} \left(\frac{t-t_0}{\sigma} - \frac{\sigma}{\tau}\right)\right) \right] + B$$

with the error function defined as

$$\text{erf}(x) = \frac{2}{\sqrt{\pi}} \int_0^x dt e^{-t^2}$$

Note that the actual amplitude of the peak is not directly read from the parameters of the fitness function but has to be calculated as follows:

$$A = \text{fit}(t_0) - B$$

The same applies for ΔT as it is a function of σ and τ (and not just a function of σ as in the Gauss curve). The optimization process results in a sensitivity high enough to regularly measure well below ppm level. Peak width decreased to 4 ns FWHM which is equal to the length of the applied laser beam on the sample. An example optimization result can be seen in Fig. 11. (Fig. 12)

DISCUSSION AND OUTLOOK

The APSO algorithm was successfully implemented as an optimization method for TOF mass spectrometers. It has been shown that for all tested instruments, an increase in performance was typically achieved within several hours of optimization.

Introduction of penalty functions is necessary to handle potential error sources that would mislead the optimization process; therefore, it is important to have knowledge of the instrument's approximate peak performance.

Although no changes are necessary to the APSO algorithm itself, boundary conditions need to be adapted individually for every instrument. Particularly, emphasis has to be put on the choice of fitness and definition of penalty functions. Definition

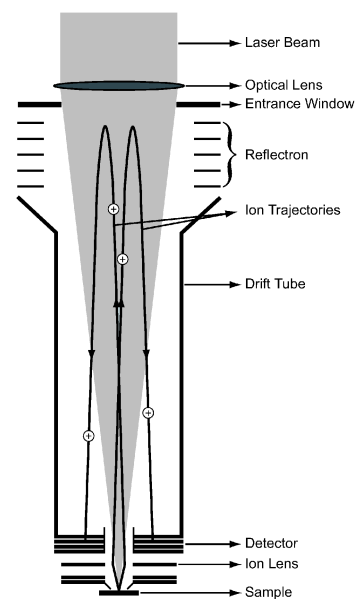


Figure 11. Overview of the LMS instrument. Incoming laser beam is denoted as the grey area and has a pulse width of 4 ns, repetition rate of 20 Hz and a wavelength of 266 nm. Figure modified from ref. [18]

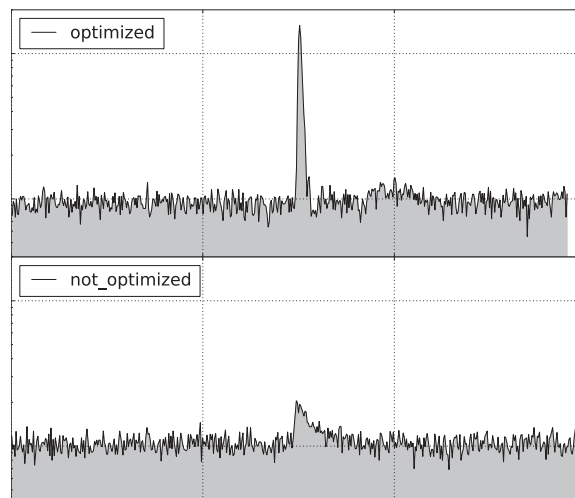


Figure 12. Na peak of a LMS measurement before and after optimization. At the beginning of the optimization process, an asymmetric peak shape can clearly be seen (lower graph) whereas the optimized peak shape is symmetric.

of a “good” solution is ambiguous if the defined fitness function is a combination from various quantities (e.g. mass resolution and sensitivity), depending on how the different aspects are weighted. Finding the right balance of all evaluated quantities is essential for an efficient optimization campaign. Promising results have been achieved with multiple stage fitness functions, where different stages are triggered by user-defined thresholds.

Currently, TOM is lacking fast electronics which results in dead times of up to 10 s between measurements where voltages for new solution candidates are updated. As dead time is of the same order of magnitude as the actual measurement, faster high voltage power supplies will substantially increase the optimization speed.

The implementation of the optimizer algorithm into the ROSINA data processing unit (DPU) is under way. It has been demonstrated that the optimizer runs the instrument for several days without any error messages from the DPU. For later application in space, absolute reliable systems are needed as a single DPU error message can compromise the two other ROSINA sensors that share the DPU with RTOF. Therefore, as a next step, a detailed series of test runs under controlled laboratory conditions on the flight spare instrument is performed. Additionally, the algorithm for RTOF is also used when the triple reflection mode is optimized. In 2014 (Currently the Rosetta space craft is in hibernation until 20.01.2014), the tested software will be uplinked to the spacecraft and be implemented into the DPU unit.

The optimization process at the LMS indicates very promising results mostly concerning instrument sensitivity and mass resolution. Currently, the set of optimization parameters is extended such that not only voltages but also the laser-probe geometry (to determine the focal point of the laser) and laser fluence are included into the optimization process.

Acknowledgements

The authors would like to thank the Canton of Bern, the Swiss National Science Foundation and the ESA PRODEX Program, which supported this work. We herewith acknowledge gratefully the work of numerous engineers from the institutions involved in ROSINA and especially from the University of Bern who contributed significantly to the ROSINA instrument and to the other mass spectrometers built in-house.

REFERENCES

- [1] H. Balsiger, P. Eberhardt, J. Geiss, A. Ghielmetti, H. P. Walker, D. T. Young, H. Loidl, H. Rosenbauer. A satellite-borne ion mass spectrometer for the energy range 0 to 16 keV. *Space Sci. Instrum.* **1976**, *2*, 499–521.
- [2] G. Gloeckler, J. Geiss, H. Balsiger, P. Bedini, J. C. Cain, J. Fischer, L. A. Fisk, A. B. Galvin, F. Gliem, D. C. Hamilton, J. V. Hollweg, F. M. Ipavich, R. Joss, S. Livi, R. Lundgren, U. Mall, J. F. McKenzie, K. W. Ogilvie, F. Ottens, W. Rieck, E. O. Tums, R. von Steiger, W. Weiss, B. Wilken. The solar wind ion composition spectrometer. *Astr. Astrophys. Suppl. Ser.* **1992**, *92*, 267–289.
- [3] H. Balsiger, K. Altwegg, P. Bochsler, P. Eberhardt, J. Fischer, S. Graf, A. Jäckel, E. Kopp, U. Langer, M. Mildner, J. Müller, T. Riesen, M. Rubin, S. Scherer, P. Wurz, S. Wüthrich, E. Arijs, S. Delanoye, J. de Keyser, E. Neefs, D. Nevejans, H. Rème, C. Aoustin, C. Mazelle, J.-L. Médale, J. A. Savaud, J.-J. Berthelier, J.-L. Bertaux, L. Duvet, J.-M. Illiano, S. A. Fuselier, A. G. Ghielmetti, T. Magoncelli, E. G. Shelley, A. Korth, K. Heerlein, H. Lauche, S. Livi, A. Loose, U. Mall, B. Wilken, F. Gliem, B. Fiethe, T. I. Gombosi, B. Block, G. R. Carignan, L. A. Fisk, J. H. Waite, D. T. Joungh, H. Wollnik. Rosina - Rosetta Orbiter Spectrometer for Ion and Neutral Analysis. *Space Sci. Rev.* **2007**, *128*, 745–801.
- [4] J. Kissel, K. Altwegg, B. C. Clark, L. Colangeli, H. Cottin, S. Czerniack, J. Eibl, C. Engrand, H. M. Fehring, B. Feuerbacher, M. Fomenkova, A. Glasmachers, J. M. Greenberg, E. Grün, G. Haerendel, H. Henkel, M. Hilchenbach, H. von Hoerner, H. Höfner, K. Hornung, E. K. Jessberger, A. Koch, H. Krüger, Y. Langevin, P. Parigger, F. Raulin, F. Rüdener, J. Rynö, E. R. Schmid, R. Schulz, J. Silén, W. Steiger, T. Stephan, L. Thirkell, R. Thomas, K. Torkar, N. G. Utterback, K. Varnuza, K. P. Wanczek, W. Werther, H. Zscheeg. COSIMA – High Resolution Time-of-Flight Secondary Ion Mass Spectrometer for the Analysis of Cometary Dust Particles Onboard Rosetta. *Space Sci. Rev.* **2007**, *128*, 823–867.
- [5] H. B. Niemann, S. K. Atreya, S. J. Bauer, K. Biemann, B. Block, G. R. Carignan, T. M. Donahue, R. L. Frost, D. Gautier, J. A. Haberman, D. Harpold, D. M. Hunten, G. Israel, J. I. Lunine, K. Mauersberger, T. C. Owen, F. Raulin, J. E. Richards, S. H. Way. The Gas Chromatograph Mass Spectrometer for the Huygens Probe. *Space Sci. Rev.* **2002**, *104*(1), 553–591.
- [6] J. H. Waite Jr., W. S. Lewis, W. T. Kasparzak, V. G. Anicich, B. P. Block, T. E. Cravens, G. G. Fletcher, W. -H. Ip, J. G. Luhmann, R. L. McNutt, H. B. Niemann, J. K. Parejko, J. E. Richards, R. L. Thorpe, E. M. Walter, R. V. Yelle. The Cassini ion and neutral mass spectrometer (INMS) investigation. *Space Sci. Rev.* **2004**, *114*(1), 113.
- [7] A. Morse, A. Geraint, D. Andrews, S. Barber, M. Leese, S. Sheridan, I. Wright, C. Pillinger. Ptolemy - a GCMS to measure the chemical and stable isotopic composition of a comet. In *Rosetta ESA's Mission to the Origin of the Solar System*, R. Schulz, H. Boehnhardt (Eds). Springer: Berlin/Heidelberg, **2009**, 669–718.
- [8] F. Goesmann, H. Rosenbauer, R. Roll, C. Szopa, F. Raulin, R. Sternberg, G. Israel, U. Meierhenrich, W. Thiemann, G. Muñoz-Caro. Cosac, The Cometary Sampling and Composition Experiment on Philae. *Space Sci. Rev.* **2007**, *128*(1), 257–280.
- [9] G. G. Managadze, P. Wurz, R. Z. Sagdeev, A. E. Chumiko, M. Tulej, M. Yakovleva, N. G. Managadze, A. L. Bondarenko. Study of Main Geochemical Characteristics of Phobos's Regolith Using Laser Time-of-Flight Mass Spectrometry. *Sol. Syst. Res.* **2010**, *44*(5), 376–384.
- [10] G. G. Managadze, I. Y. Shutyaev. *Chemical Analysis*, Wiley: New York, **1993**, 124.
- [11] W. B. Brinckerhoff, G. G. Managadze, R. W. McEntire, A. F. Cheng, W. J. Green. Laser time-of-flight mass spectrometry for space. *Rev. Sci. Instrum.* **2000**, *71*, 536–545.
- [12] L. M. Zelenyi, A. V. Zakharov. Phobos_Grunt Project: Devices for Scientific Studies. *Sol. Syst. Res.* **2010**, *44*(5), 359–361.
- [13] J. Kennedy, R. C. Eberhart. Particle swarm optimization. *Proc. IEEE Int. Conf. Neural Netw., Perth, Australia* **1995**, *4*, 1942–1948.
- [14] Z.-H. Zhan, J. Zhang, Y. Li, H. S.-H. Chung. Adaptive particle swarm optimization. *IEEE Trans. Syst. Man Cybern. B Cybern.* **2009**, *39*(6), 1362–1381.
- [15] A. Bieler. PhD Thesis to be published, University of Bern, Switzerland, **2012**.
- [16] P. Wurz, L. Gubler. Impedance-Matching Anode for Fast Timing Detectors. *Rev. Sci. Instrum.* **1994**, *65*, 871–876.
- [17] P. Wurz, L. Gubler. Fast Micro-Channelplate Detector for Particles. *Rev. Sci. Instrum.* **1996**, *67*, 1790–1793.
- [18] M. Tulej, M. Iakovleva, I. Leya, P. Wurz. A miniature mass analyzer for in-situ elemental analysis of planetary material – performance studies. *Anal. Bioanal. Chem.* **2010**, *399*, 2185–2200.